Space Weather

RESEARCH ARTICLE
10.1029/2022SW003105

# Variations in Observations of Geosynchronous Magnetopause and Last Closed Drift Shell Crossings With Magnetic Local Time

**Thomas A. Daggitt[1,2], Richard B. Horne[1], Sarah A. Glauert[1], Giulio Del Zanna[2], and Mervyn P. Freeman[1]**

[1]British Antartic Survey, Cambridge, UK, [2]Department of Applied Mathematics and Theoretical Physics, University of Cambridge, Cambridge, UK

**Key Points:**

- Last closed drift shell models based on TS05 and TS07 fields underpredicted and occasionally overpredicted brief magnetopause crossings
- Geostationary satellites only 4 hr apart in magnetic local time may see different flux profiles for events with geosynchronous magnetopause crossings
- Fluxes observed on the nightside may be unrepresentative of dayside conditions showing the need for greater longitudinal satellite coverage

**Correspondence to:**
T. A. Daggitt,
thoggi18@bas.ac.uk

**Citation:**
Daggitt, T. A., Horne, R. B., Glauert, S. A., Del Zanna, G., & Freeman, M. P. (2022). Variations in observations of geosynchronous magnetopause and last closed drift shell crossings with magnetic local time. *Space Weather*, *20*, e2022SW003105. https://doi.org/10.1029/2022SW003105

Received 25 MAR 2022
Accepted 8 JUN 2022



**Abstract** We analyze a set of events in which both electron flux dropouts caused by magnetopause shadowing and geosynchronous magnetopause crossings (GMCs) are observed. These observations are compared to event-specific last closed drift shell (LCDS) models derived from the TS05 and TS07 external field models and magnetopause standoff distance. The LCDS models show good association with losses due to magnetopause shadowing but fail to reproduce observations of GMCs on the timescale of minutes. We show that different satellites in geostationary orbit observe different trends in electron flux during storm events on timescales of less than a day due to their separation in longitude. These differences demonstrate that both satellite $L^*$ and magnetic local time must be taken into account when modeling rapid variations in the outer radiation belt, and at least three satellites in geostationary orbit, ideally more, may be required for accurate forecasting and reconstruction of these events on timescales shorter than days.

**Plain Language Summary** We analyze a set of events in which the number of electrons trapped in Earth's outer radiation belts drops rapidly due to inward movement of the outer edge of Earth's magnetic field. These observations are compared to models of the outermost trapped electron orbits derived from models of Earth's magnetic field and particle tracing models. These models of the largest trapped orbits agree well with the losses seen over the timescale of hours but fail to reproduce more rapid decreases in the number of electrons measured on the timescale of minutes. We show that different satellites in geostationary orbit observe different trends in the trapped electron population on timescales of less than a day during geomagnetic storms due to their separation in longitude. These differences demonstrate that data from at least three satellites in geostationary orbit, ideally more, may be required for accurate, high time resolution forecasting and reconstruction of Earth's radiation belts during geomagnetic storms.

## 1. Introduction

Earth's radiation belts are comprised of high energy charge particles trapped by Earth's magnetic field (Van Allen & Frank, 1959). This high radiation environment presents a hazard to satellites operating within it, as high energy charged particles can cause charging and subsequent discharging within electronic components, damaging satellites (Wrenn, 1995). Many satellites providing crucial communications and research infrastructure are in geostationary orbit, near the outer edge of the highly variable outer radiation belt. As such it is important to understand the processes driving the variability of the outer radiation belt.

Some of the most rapid variations in electron fluxes observed in the outer radiation belt are electron flux dropouts, which are order of magnitude reductions in flux over a range of L shells and energies within timescales of hours (Morley et al., 2010; Turner et al., 2012). High energy electron flux losses in the outer radiation belts can be caused by both losses to the magnetopause (Olifer et al., 2018; Shprits et al., 2006) and atmospheric precipitation caused by interaction with EMIC and chorus waves (Capannolo et al., 2019; Shprits et al., 2016). In the case of electron flux dropouts during intense storm events, it has been shown that losses to the magnetopause can dominate at large $L^*$ (Tu et al., 2019; Yu et al., 2013). This mechanism is known as magnetopause shadowing, where previously closed drift paths become open due to the inward motion of the magnetopause. Electrons on these drift paths will intersect the magnetopause and be lost within one drift orbit. These losses create a steep gradient in electron phase space density which results in more electrons diffusing onto open paths due to outward transport processes, propagating losses further in the radiation belts (Loto'Aniu et al., 2010).

The outermost drift path that does not intersect with the magnetopause is known as the last closed drift shell (LCDS). The LCDS lies within the magnetopause and represents the boundary beyond which there is no flux trapped by Earth's inner magnetosphere. Sufficiently high solar wind dynamic pressure coupled with an extended period of southward interplanetary magnetic field (IMF) can bring the magnetopause within geostationary orbit temporarily, which may be detected by geostationary satellites, though these geosynchronous magnetopause crossings (GMCs) are rare (Rufenach et al., 1989). Satellites crossing the magnetopause will see a sudden change in magnetic field strength and direction as they move out of Earth's magnetic field, coupled with a rapid decrease in the measured flux as the satellites will no longer encounter any significant levels of trapped flux. Data from geostationary satellites such as the GOES-13 and GOES-15 satellites are commonly used as boundary conditions for models of the outer radiation belts, for example, S. A. Glauert et al. (2018) and Wang and Shprits (2019). In order to capture the effect of GMCs on the outer radiation belts, Wang and Shprits (2019) set the phase space density outside the LCDS to zero when the LCDS is determined to be within the outer boundary, and S. A. Glauert et al. (2018) use a loss term inversely proportional to the drift period for phase space density outside the LCDS. In cases where the LCDS model used for these methods does not accurately reflect the location of the LCDS, extra losses may be artificially introduced or the boundary conditions may be derived from measurements taken outside the radiation belts. Any variation in how the LCDS position is determined and in how its effects are modeled may result in different reproductions of GMCs by radiation belt models. As such it is important to understand the link between sudden drops in measured flux caused by LCDS crossings and losses in trapped flux caused by magnetopause shadowing.

In this paper, we investigate three roughly 15 hr time periods involving GMCs using electron flux data from the GOES-13, GOES-15, and Himawari-8 geostationary satellites and three different LCDS models. As many approaches to modeling, the outer radiation belts use an LCDS time series to model losses to the magnetopause (S. A. Glauert et al., 2014; Tu et al., 2019). We compare the performance of three LCDS models in predicting both flux dropouts and LCDS crossings. We also investigate the extent to which choice of satellite may impact the observation of an event involving GMCs. Under more or less extreme solar wind conditions, GMCs can vary in timescale from under a minute to hours (Rufenach et al., 1989), comparable or less than the drift period of high energy electrons near the magnetopause. As a result, observations of GMCs may be dependent on satellite location at the exact time of the GMC and may provide unreliable information about fluxes at other magnetic local times (MLTs) during or after the crossing.

## 2. Data and Methodology

Solar wind dynamic pressure and IMF magnitude and Geocentric Solar Magnetospheric (GSM) z component were taken from the OMNIWeb database. This was compared to 1 min resolution magnetic field data from the GOES-13 and GOES-15 magnetometers, and 1 min resolution integral flux data from the GOES Energetic Proton, Electron, and Alpha Detector (EPEAD) for electrons with energy >0.8 MeV. The GOES-13 and 15 satellites were in geostationary orbit at 75° and 135° west geographic longitude, respectively. These data were compared to LCDS models based on the TS05 and TS07 external magnetic field models (Tsyganenko & Sitnov, 2005, 2007), implemented using the International Radiation Belt Environment Modeling (IRBEM) library (Boscher et al., 2013). The LCDS location was determined according to the method from Albert et al. (2018) as the largest value of the Roederer $L^*$ (Roederer, 1970) returned by IRBEM when searching radially outward, staying on the magnetic equator, at 12:00 MLT at any given time. The satellite $L^*$ values were also determined using the same field model for comparison to the LCDS models. All $L^*$ and LCDS values were calculated at 1 min intervals for each event. These LCDS models are presented alongside a model of the LCDS position based on the Shue magnetopause (Shue et al., 1998) currently used in the British Antarctic Survey Radiation Belt Model (S. A. Glauert et al., 2014) to model losses to the magnetopause. This model shall be referred to as the Gl14 model. The Gl14 LCDS position is determined by first applying a $1R_E$ correction to the standoff distance of the Shue magnetopause, according to the results shown by Case and Wild (2013), then applying a linear displacement from this position based on particle tracing simulations done by Matsumura et al. (2011). The magnetopause standoff distance in $R_E$ is given by the model from Shue et al. (1998):

$$r_0 = [10.22 + 1.29\tanh(0.184\,(B_z + 8.14))]\,(D_p)^{-\frac{1}{6.6}} \quad (1)$$

where the $D_p$ is the solar wind dynamic pressure in nPa and $B_z$ is the $z$ component of the IMF in GSM coordinates. The $L^*$ for this LCDS model is thus given by the following equation:

$$L^*_{LCDS}(\alpha) = (r_0 - 1)\,(1.6375 - 0.00975\alpha) + 0.05387\alpha - 4.8937 \quad (2)$$

where $\alpha$ is the equatorial pitch angle in degrees. For electrons with a pitch angle of 90°, this reduces to

$$L^*_{LCDS}(90) = 0.7591\,(r_0 - 1) - 0.0454 \quad (3)$$

All LCDS and $L^*$ values were calculated for electrons with an equatorial pitch angle of 90°, as it is assumed that the field of view of the GOES EPEAD is dominated by near equatorially mirroring electrons. None of the LCDS models are energy dependent, and thus any effects caused by varying electron gyroradius are not considered. Data from the Himawari-8 SEDA-e high energy electron sensor were also used for the later two events, during which these data were available. The Himawari-8 satellite is in geostationary orbit at 140° east and provides a partial view of the nightside flux while the GOES satellites are on the dayside.

To find time periods for this paper, the GOES-13 and GOES-15 magnetometer data sets were searched from 1 January 2011 to 14 December 2017 for potential magnetopause crossings using the method for the Geotail satellite from Case & Wild (2013), slightly adapted for use with the GOES data set. The 3 minute rolling means and standard deviations of $|B|$ and $B_z$ were calculated, and each value was compared to the value in 3 minutes time. A potential crossing from the magnetosphere into the magnetosheath was recorded if these values satisfied the following criteria:

1. The standard deviation of $|B|$ in the magnetosheath must be less than 4.5 nT and more than 2.5 times the standard deviation of $|B|$ in the magnetosphere
2. The mean $B_z$ within the magnetosphere must be more than 1.3 times the mean $B_z$ in the magnetosheath

The results were visually inspected, and the only events kept were those with clear GMCs, where both satellites were on the dayside ($6 < \text{MLT} < 18$) and clear evidence of drops in measured flux were observed simultaneous with the crossings. This left 10 events. This is a fairly small number of events over a seven year period, compared to the 64 events found by Rufenach et al. (1989) from 1978 to 1986. This reduction can be partially explained by the strict criteria, requiring observations of magnetopause crossings to be on the dayside, with associated drops in measured flux. Any further reduction may be attributable to the relative strength of solar cycles 21 and 24 (McIntosh et al., 2020). The requirement for the GOES satellites to be on dayside was put in place to avoid variation in the measured flux and magnetic field caused by distortion of the magnetotail (Capannolo et al., 2022; Green et al., 2004). From these 10 events, the three time periods chosen for analysis were the 27 February 2014, 22 June 2015, and 14 December 2015.

## 3. Event Analysis

### 3.1. 27 February 2014 Event

Figure 1 shows the storm spanning 27–28 February 2014. The storm begins with a spike in solar wind pressure at 17:00, with the solar wind pressure remaining elevated above quiet time levels of <5nPA for several hours afterward. The IMF $B_z$ is southward for the initial shock and for most of the period afterward. The combined effect of compression of the magnetopause by the solar wind and erosion of the dayside flux by the southward IMF is expected to result in inward movement of the magnetopause. Panels (C) and (D) show increases in the magnetic field strength at the GOES satellites at the time of the initial shock, caused by compression of the dayside field. This effect is more apparent in the GOES-13 data, as GOES-13 is near noon at this time, whereas GOES-15 is on the flank, closer to dawn as seen in panel (H). Shortly after the initial shock, GOES-13 shows a brief period of strongly negative $B_z$, reaching −80 nT, indicating a short GMC lasting under 2 min, going by the length of time for which $B_z$ is negative. This is supported by the measured flux in panel (G), which shows a dip of two orders of magnitude for GOES-13 at this time, suggesting that GOES-13 is no longer measuring any trapped flux at this time. GOES-15 does not see a GMC at this time, likely because it is further from noon. At this time both the TS05 and TS07 models place GOES-15 at a higher $L^*$ than GOES-13 in panels (E) and (F), but the observational data suggest that GOES-13 crosses the LCDS at 17:00 while GOES-15 does not. This suggests that the change in the external magnetic field during this GMC is too rapid to be modeled by the TS05 and TS07 models. This is

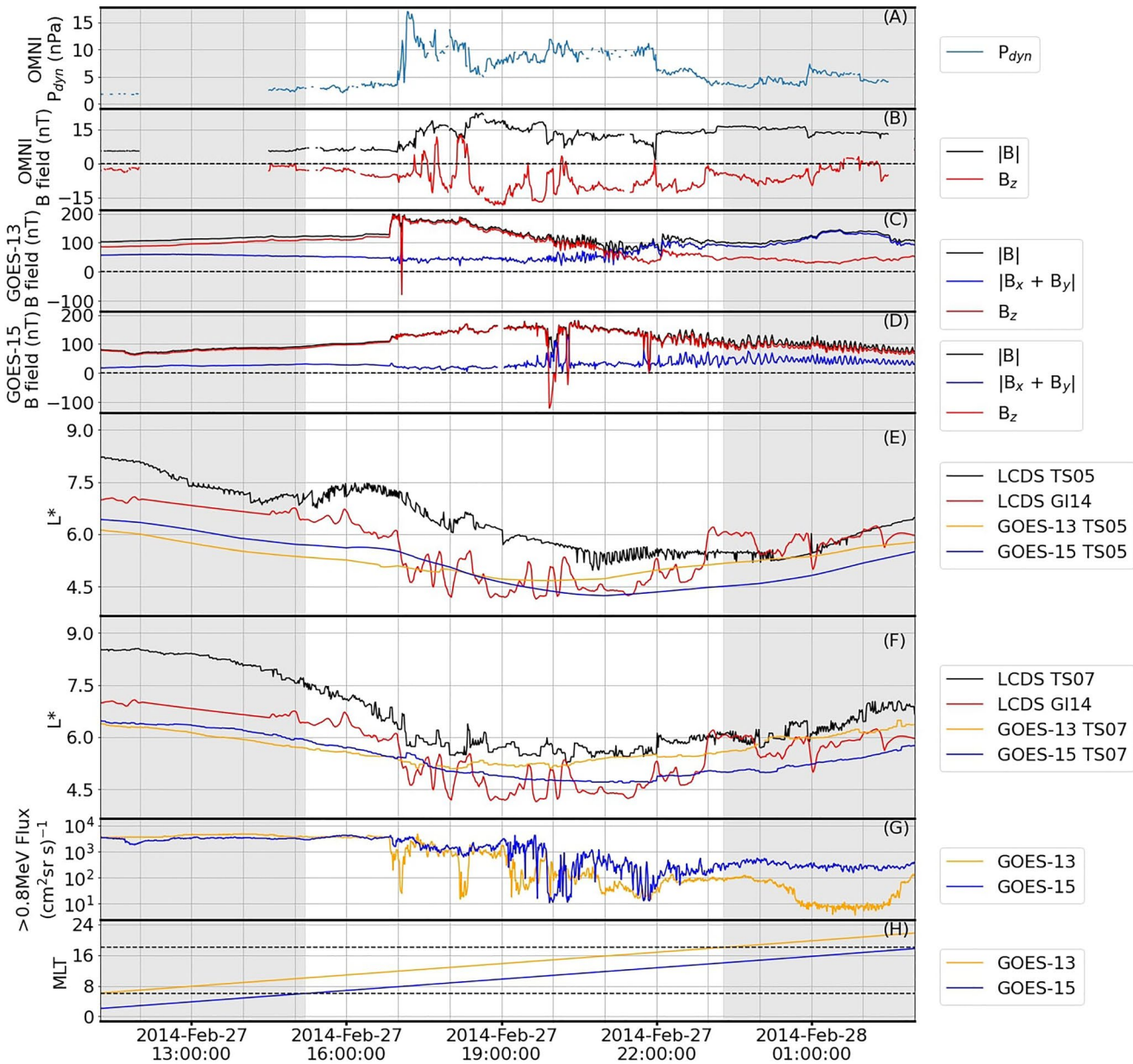


**Figure 1.** Storm event on 27–28 February 2014. Panels (a and b) show the solar wind dynamic pressure and interplanetary magnetic field magnitude and Geocentric Solar Magnetospheric (GSM) $z$ component from the OMNIWeb database. Panels (c and d) show the **B** field magnitude, GSM $z$ component, and component in the ($x$, $y$) plane from the GOES-13 and 15 satellites. Panels (e and f) show the satellite and last closed drift shell (LCDS) $L^*$ for the TS05 and TS07 field models, along with the LCDS given by Equation 2. Panel (g) shows the >0.8 MeV integral flux from the GOES Energetic Proton, Electron, and Alpha Detector instruments. Panel (h) shows the MLT of the GOES satellites. Times when one or both of the satellites are on the nightside ($6 < MLT < 18$) are shown by the darker shaded region.

supported by the LCDS models, which do not show any satellite LCDS crossings or even any significant response to this GMC.

A second similar dip in the GOES-13 flux occurs at 18:10. This dip is associated with a second smaller peak in solar wind pressure, but the IMF turns northward during this dip. It is unclear exactly what caused this dip in flux. The magnitude of the dip suggests that it may be a second magnetopause crossing, with the northward direction of the IMF explaining the lack of negative $B_z$ seen by the GOES-13 magnetometer. However, this is contradictory to the expected magnetopause standoff distance, which should be greater than at 17:00, when the solar wind pressure was higher and the IMF was southward. Other possible explanations for this dip are a magnetopause crossing

at a slightly later MLT that was not observed directly causing rapid losses that propagate to GOES-13 or close proximity to the magnetopause without crossing it causing rapid losses due to radial diffusion.

At 19:00 the flux measured by both GOES satellites becomes highly variable and begins to drop by two orders of magnitude over the next 3 hours. During this time, both TS05 and TS07, and the Gl14 LCDS model show that the distance between the satellites and the LCDS has shrunk to roughly half the distance before the solar wind peak. During this time the $L^*$ of GOES-13 remains roughly constant, while GOES-15 drops in $L^*$. The losses are more rapid for GOES-13 at higher $L^*$. This is consistent with losses caused by magnetopause shadowing propagating to lower $L$ shells due to radial diffusion down the phase space gradient. During this time GOES-15 observes a longer GMC lasting 5 min at 20:00 that is not seen by GOES-13, demonstrated by the longer period of strongly negative $B_z$ and dip in flux observed by GOES-15. This is closely followed by a second shorter GMC, less than 2 min in length. At this point GOES-15 is now closer to noon than GOES-13, resulting in only GOES-15 observing the crossings. This roughly 5 min period is the longest period of negative $B_z$ at a GOES satellite for which neither field model based LCDS model shows a crossing. By 03:00 28 February, at the end of the plotted time period, the flux at both satellites has dropped by over an order of magnitude compared to before the event 12:00 27 February. The field models both indicate that the satellites end the plotted period at similar $L^*$ values to which they started. This drop in flux thus represents a loss of trapped electrons over the course of the event. GOES-13 ends at a higher $L^*$ and records a greater net loss of flux. The drop in flux over a range of $L^*$ values suggests that flux has been lost due to a combination of direct magnetopause shadowing and radial diffusion outward from lower $L^*$.

The TS05 and TS07 LCDS models behave similarly during this event, both move inward in response to increases in solar wind pressure and sustained southward IMF, and both come into close proximity to the satellites while losses are occurring, consistent with the expected losses to magnetopause shadowing. However, the only times when the LCDS models and satellite $L^*$ values cross are later in the event, around 00:00 28 February for both models. These crossing predictions are not associated with an observation of a GMC in the satellite data. The main difference between the TS05 and TS07 LCDS models in this event is the rapid $\approx 0.5 R_E$ fluctuations seen in the TS05 model while the LCDS model is at its lowest. The Gl14 LCDS model is significantly lower than the TS05 and TS07 models for most of the event. It does predict LCDS crossings at 17:00 for both satellites but continues to predict crossings for both satellites frequently for the rest of the event. Only some of these are associated with reductions in the measured flux at the satellites. In particular, around 19:00 the Gl14 model suggests that both satellites should be outside the LCDS for roughly 30 min but the fluxes at GOES-15 remain high. In this event the Gl14 LCDS performs better than the TS05 and TS07 models at predicting LCDS crossings associated with the observed GMCs but overall seems to predict LCDS crossings at an excessive rate. This suggests that it may be underestimating the LCDS position and thus is doing worse than the TS05 and TS07 field models at predicting the overall trends in the measured flux.

After 22:20 GOES-13 passes onto the nightside, shown by the darker shaded area in Figure 1. At this time the solar wind pressure has dropped close to quiet time levels and the IMF is only weakly southward. The flux at GOES-15 has begun to increase, while its $L^*$ also increases. This suggests that recovery phase of the event has begun. Starting at 00:30 28 February, GOES-13 shows a large drop in measured flux lasting roughly two hours that is not seen by GOES-15. The large component of the magnetic field in the $(x, y)$ plane seen by GOES-13 on the nightside, but not by GOES-15 on the dayside, indicates that this drop is caused by tail stretching.

### 3.2. 22 June 2015 Event

The event shown in Figure 2 contained the longest lasting GMC out of all of the events considered. The solar wind pressure for this event is relatively high at the beginning of the period shown compared to the other events, staying near 8 nPa for the 8 hours before the large peak of 60 nPa at 18:40. This higher pressure before the event explains the proximity of the TS05 and TS07 LCDS models to the satellite $L^*$ values even before the arrival of the shock. Combined with the expected higher variance in observed electron fluxes on the nightside compared to the dayside, this proximity explains the variations in the flux recorded by the GOES satellites during this time. For this event, the 1 MeV differential flux from the Himawari-8 SEDA-e instrument is shown alongside the integral flux from the GOES EPEAD instruments in panel (G). Work by Nagatsuma et al. (2017) showed that the GOES EPEAD integral flux, when converted to 1 MeV differential flux, was in good agreement with the SEDA-e instrument. As we are more interested in trends in flux than absolute values in this study, no conversion has been performed for these events.

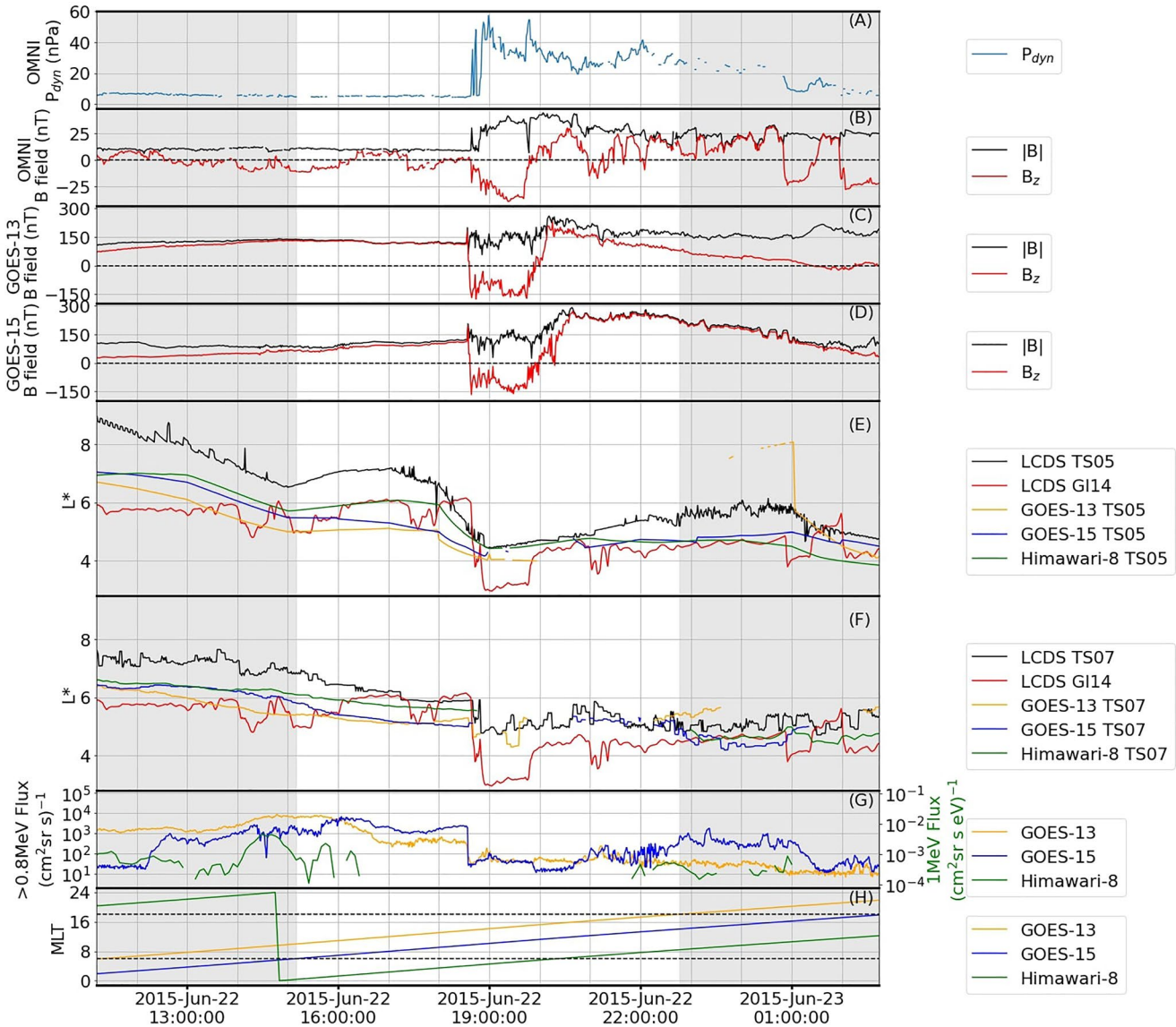


**Figure 2.** Storm event on 22–23 June 2015. Panels (a and b) show the solar wind dynamic pressure and interplanetary magnetic field magnitude and Geocentric Solar Magnetospheric (GSM) $z$ component from the OMNIWeb database. Panels (c and d) show the **B** field magnitude, GSM $z$ component, and component in the ($x$, $y$) plane from the GOES-13 and 15 satellites. Panels (e and f) show the satellite and last closed drift shell (LCDS) $L^*$ for the TS05 and TS07 field models, along with the LCDS given by Equation 2. Panel (g) shows the >0.8 MeV integral flux from the GOES Energetic Proton, Electron, and Alpha Detector instruments and the 1 MeV differential flux from the Himawari-8 SEDA-e instrument. Panel (h) shows the magnetic local time (MLT) of the satellites. Times when one or both of the satellites are on the nightside ($6 < \text{MLT} < 18$) are shown by the darker shaded region.

The peak in solar wind pressure at 18:40 is accompanied by a simultaneous switch to strongly southward IMF, with the $B_z$ component reaching −30 nT. This combination causes immediate GMCs at both GOES satellites, shown by the negative $B_z$ values recorded for the next 1.5 hr. The onset of these GMCs is accompanied by an order of magnitude drop in flux at both satellites seen in panel (G). Gradual losses due to the proximity of the LCDS prior to the GMC may have resulted in the smaller size of this drop compared to drops in the other events. During this event both the TS05 and TS07 models occasionally place the satellites at a higher $L^*$ than the LCDS, which is unphysical as the LCDS is defined as the largest possible $L^*$ for a given field configuration. Investigations of the LCDS model suggest that this is caused by a dependence on the longitude at which the radial search for the LCDS is performed, due to the effects of drift orbit bifurcation on IRBEM's drift shell tracing procedure. For this study, any period where the $L^*$ of a satellite is undefined or greater than the LCDS will be considered an LCDS crossing. The GI14 LCDS model begins the event at a lower $L^*$ than the satellites for both the TS05 and TS07

field models and predicts that all three satellites should be beyond the LCDS for the majority of the event. This is at odds with the behavior of the flux at the GOES satellites, which show relatively stable fluxes when they are on the dayside for the hours preceding the solar wind peak at 18:40. The TS05 and TS07 models only show LCDS crossings shortly after the onset of the GMC, predicting further repeated crossings for the rest of the event. The fluxes at both satellites remain low for the duration of the GMC, and the flux at GOES-15 begins to recover at around 20:30, when the magnetic field at both GOES satellites returns to north. Although the magnetometer data suggest that both satellites have crossed back into the magnetosphere, the TS05 and TS07 LCDS models and the Gl14 LCDS model all suggest that the satellites are still near or beyond the LCDS for much of the rest of the period shown. This is supported by the slow recovery in flux seen by GOES-15 as it remains near $L^* = 5$. The extremity of the GMC, in which the LCDS models reached around $L^* = 4$, may also contribute to the slow recovery, as flux at lower $L$ shells has been lost, resulting in less flux diffusing out from lower L shells. The partial recovery seen at GOES-15 is not seen at GOES-13. This is consistent with both field models showing GOES-13 at a higher $L^*$ or beyond the LCDS for a longer time. This may also be due to GOES-13 moving onto the nightside earlier, and seeing lower fluxes due to tail stretching in the magnetotail, as seen in Figure 1. Panel (C) in Figure 2 shows a large component of the magnetic field in the ($x$, $y$) plane at GOES-13 after 20:00 22 June, not seen by GOES-15 until after 2:00 23 June. This same effect is seen at the GOES-15 satellite while it is on the nightside at 12:00 22 June. The TS05 model also shows evidence of very unusual behavior on the nightside, placing GOES-13 at $L^* = 8$ for several discontinuous minutes around 1:00 23 June during another period of strongly southward IMF. This is well above the LCDS location, and above the range of the usual quiet time $L^*$ of GOES-13. During this event, the TS07 model does return $L^*$ values above the LCDS for longer than the TS05 model but only by a very small margin. The Gl14 LCDS model underestimates the position of the LCDS for most of the period, predicting extended GMCs both prior to and after the observed GMC. The model does drop rapidly at the onset of the observed GMC, and recovers as the observed $B_z$ returns to positive, but overall seems to be too low for the entire event.

The Himawari-8 satellite is on the nightside for most of the period shown. Prior to the GMC, it is at a higher $L^*$ than the GOES satellites, closer to the LCDS. During this time the flux recorded by Himawari-8 is far more variable than the flux at the GOES satellites and is unrepresentative of the conditions seen by the GOES satellites on the dayside before the GMC. The high variation in recorded flux makes it difficult to tell if the Himawari-8 satellite has recorded the same net drop in flux seen by the GOES satellites over the course of the event.

### 3.3. 14 December 2015 Event

In contrast to the previous two events where there was a sudden increase in solar wind pressure, in this event the solar wind pressure rises gradually over the course of 7 hr, shown in Figure 3. Three peaks in solar wind pressure occur at 17:00, 18:00, and 18:40 14 December. The IMF is southward during each of these peaks, but the magnitude of the z component decreases for each subsequent peak. Each of these peaks is associated with brief periods of negative $B_z$ measured at GOES-13, along with drops in measured flux of 2–3 orders of magnitude. GOES-15 observes small increases in magnetic field strength during the latter two peaks, along with much smaller dips in the observed flux. It is apparent from this that GOES-13 experiences three separate GMCs, none of which are directly observed by GOES-15, which is further from noon and further westward for all of them. These GMCs all last less than 3 min based on the length of time for which GOES-15 records negative $B_z$ values. The two reductions in flux seen by GOES-15 may be caused by losses due to magnetopause shadowing propagating along the drift orbit from dusk to dawn, as the satellites are at very similar $L^*$ at this time. For electrons near 1 MeV and a 4-hr difference in MLT between GOES-13 and GOES-15, this propagation should take around 100 s, explaining the near simultaneity of the observations of flux dropouts. Alternatively, these reductions may be caused by proximity to the magnetopause, without crossing it. Near to the magnetopause, the satellite would see an increase in field strength caused by the magnetopause current, as seen in panel (D) in Figure 3. This proximity to the magnetopause and thus the LCDS coupled with high rates of radial diffusion at high $L^*$ during a high activity period may produce these rapid losses. This could explain the lack of any reduction in flux at GOES-15 during the first GMC, as there is no associated change in field strength at the satellite, suggesting that the satellite may not be as close to the LCDS as it is in the later GMCs. All three crossings are very brief, on the order of 1 minute, and are not properly predicted by the any of the LCDS models.

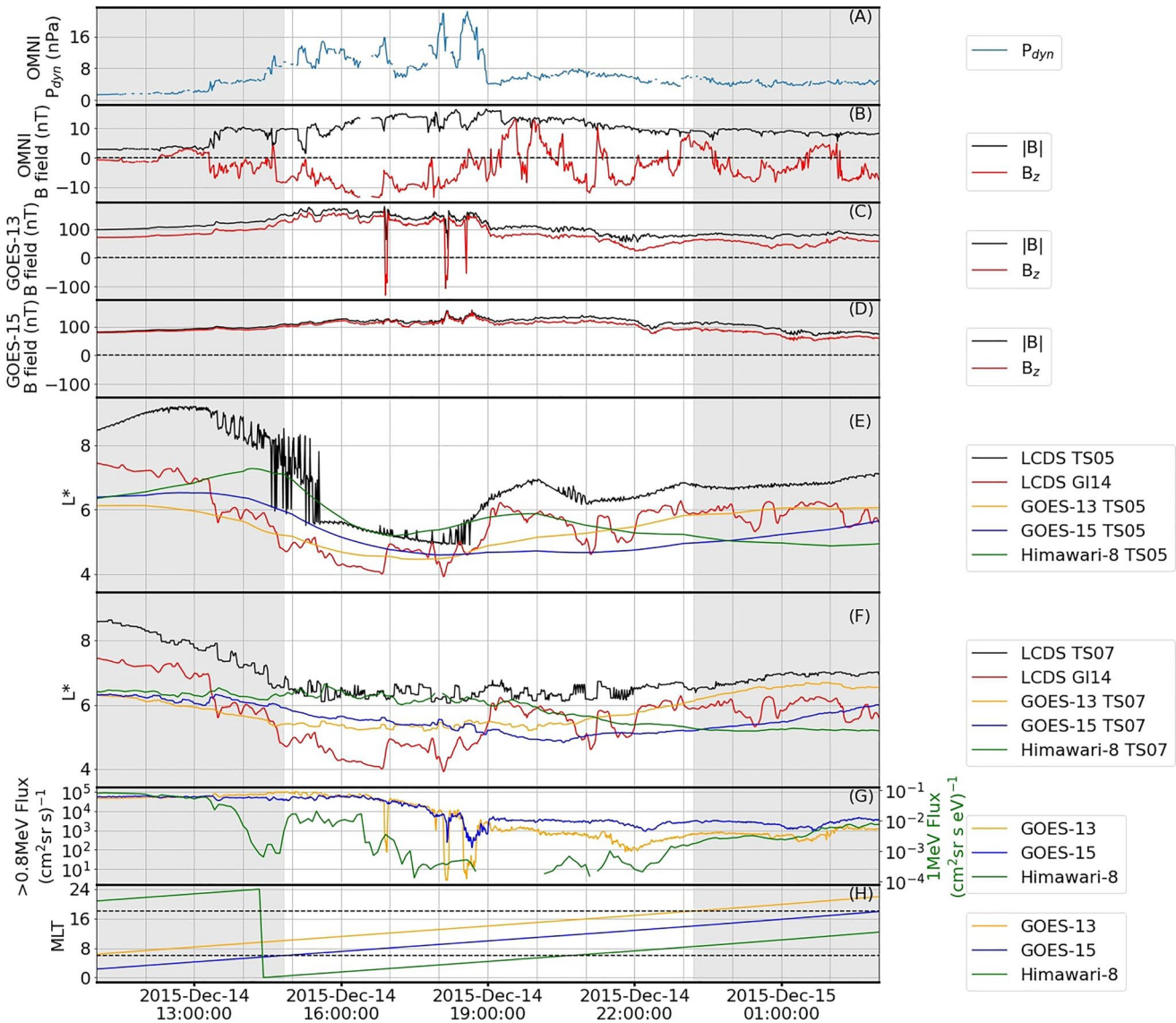


**Figure 3.** Storm event on 14–15 December 2015. Panels (a and b) show the solar wind dynamic pressure and interplanetary magnetic field (IMF) magnitude and Geocentric Solar Magnetospheric (GSM) $z$ component from the OMNIWeb database. Panels (c and d) show the **B** field magnitude and GSM $z$ component from the GOES-13 and 15 satellites. Panels (e and f) show the satellite and last closed drift shell (LCDS) $L^*$ for the TS05 and TS07 field models, along with the LCDS given by Equation 2. Panel (g) shows the >0.8 MeV integral flux from the GOES Energetic Proton, Electron, and Alpha Detector instruments and the 1 MeV differential flux from the Himawari-8 SEDA-e instrument. Panel (h) shows the magnetic local time (MLT) of the satellites. Times when one or both of the satellites are on the nightside ($6 < \text{MLT} < 18$) are shown by the darker shaded region.

The movement of the LCDS models prior to the first GMC clearly demonstrates the effect of satellite $L^*$ on how the onset of the storm is observed. The GOES satellites remain relatively close to each other in $L^*$ and observe a slow drop in flux beginning around 16:00. As the $L^*$ values of the satellites are decreasing, this drop in measured flux can be taken to imply loss of flux, either due to outward radial diffusion caused by the inward movement of the magnetopause or losses due to increased wave activity. Himawari-8 begins the period on the nightside and experiences an extended dip in flux near local midnight. The TS05 model shows that the satellite rises in $L^*$ and nears the LCDS at this time, and thus this may be due to a combination of moving to a higher $L^*$ and magnetopause shadowing. In contrast, the TS07 model shows that Himawari-8 is close in $L^*$ to the GOES satellites that do not observe this dip, suggesting that it may be caused by distortions of the magnetotail. More information is needed to determine exactly what caused this change in flux. Between 12:00 and 19:00 the flux at Himawari-8 drops by around three orders of magnitude, to the point at which it is no longer reliably recorded. This drop is

much steeper than the drop observed by the GOES satellites, which both field models place at a lower $L^*$ than Himawari-8.

The TS05 LCDS model shows large fluctuations at around 16:00 and 19:00. Similar smaller fluctuations are seen in panel (E) of Figure 1. It is not entirely clear what causes these fluctuations, but they are not seen in the TS07 model, and do not appear to affect the $L^*$ calculations at the satellites. The lack of any associated features in the solar wind and magnetic field data suggest that this may be an issue with either the field model or IRBEM's drift shell tracing procedure, or the interaction of both. The TS05 model and the TS07 model diverge more in this event than in the others, with the TS05 model showing lower $L^*$ values for both the satellites and the LCDS during the period of greatest compression, $\approx 0.5 R_E$ at 18:00 14 December. The difference between the satellites and the LCDS at the points of closest approach are similar between the two models, implying that the models should predict similar levels of magnetopause shadowing. The Gl14 LCDS model is significantly lower than both the TS05 and TS07 models for most of this event, and predicts an extended LCDS crossing for all three satellites from 13:30 to 19:00, with further repeated crossings for GOES-13 for the rest of the period shown. The lack of any extended drops in flux corresponding with these extended predicted crossings implies that the Gl14 LCDS model is underestimating the LCDS position for most of this event.

After the GMCs, the solar wind pressure remains elevated for the rest of the period shown, resulting in the TS05 and TS07 LCDS models staying at a lower $L^*$ for the rest of the period shown. The flux observed at the GOES satellites does not increase after 19:00, while the satellites increase in $L^*$. This is consistent with a slow or delayed recovery caused by continuous losses across the lowered LCDS. Both field models suggest that the GOES satellites end at a similar $L^*$ to where they began and thus that flux has been lost over the event. The increase in flux seen by Himawari-8 after the GMCs is likely due to the drop in $L^*$ from 20:00 14 December to 03:00 15 December. Unlike the other two events studied, neither GOES satellite shows any significant variation in flux compared to the other while it is on the nightside. As the $B_z$ component of the magnetic field at each satellite tracks the **B** field magnitude in panels (C) and (D) of Figure 3, it can be seen that there is no significant component of the field in the ($x$, $y$) plane when either satellite is on the nightside. This suggests that it may be possible to use the magnitude of the ($x$, $y$) relative to the $z$ component as an indicator of the uncertainty in how representative data from the nightside is of dayside conditions.

## 4. Discussion

Both flux dropouts over the course of hours and briefer observations of lower fluxes lasting between minutes and an hour were observed at geostationary orbit during multiple events. The longer flux dropouts were consistent with descriptions of relativistic electron losses caused by magnetopause shadowing mentioned in the recent work (Staples et al., 2021; Tu et al., 2019). The shorter timescale reductions in flux were associated with evidence of magnetopause crossings. LCDS models based on the TS05 and TS07 external field models and an LCDS model used with the British Antarctic Survey Radiation Belt Model were compared to relativistic electron flux and magnetic field data time series for these events from multiple satellites.

During some of these events, both the TS05 and TS07 external magnetic field models returned $L^*$ values for the satellites that were higher than the LCDS position, most noticeably at 01:00 23 June 2015 in panel (E) of Figure 2. We ascribe this unphysical behavior to the effect of drift-orbit bifurcations on the IRBEM field line tracing code, which results in radial searches at different longitudes producing different LCDS values for the same point in time. Albert et al. (2018) chose to perform the radial search for the LCDS at local midnight (MLT = 24), in order to avoid any bifurcation effects during IRBEM's setup process. For this study, we have chosen to do all LCDS calculations at local noon (MLT = 12). The reason for this is that it allows rapid, reliable identification of when an $L^*$ calculation is affected by drift-orbit bifurcation, simply by checking the number of field strength minima along the field line passing through the point at which the calculation is performed. Although Ukhorskiy et al. (2014) showed that drift orbit bifurcation can lead to increased losses for equatorially mirroring electrons at high $L^*$, we consider bifurcating drift shells to be closed as such losses occur over the course of several drift orbits, on a longer timescale than the losses considered in this study. The variations caused by searching at different MLT were not systematic, and varied with time, thus we expect the choice of search location to have no systematic effect on this study. The IRBEM code calculates $L^*$ at a given point by tracing the field line through that point and finding the second invariant for a particle with a given pitch angle on that field line. It then finds other field lines with the

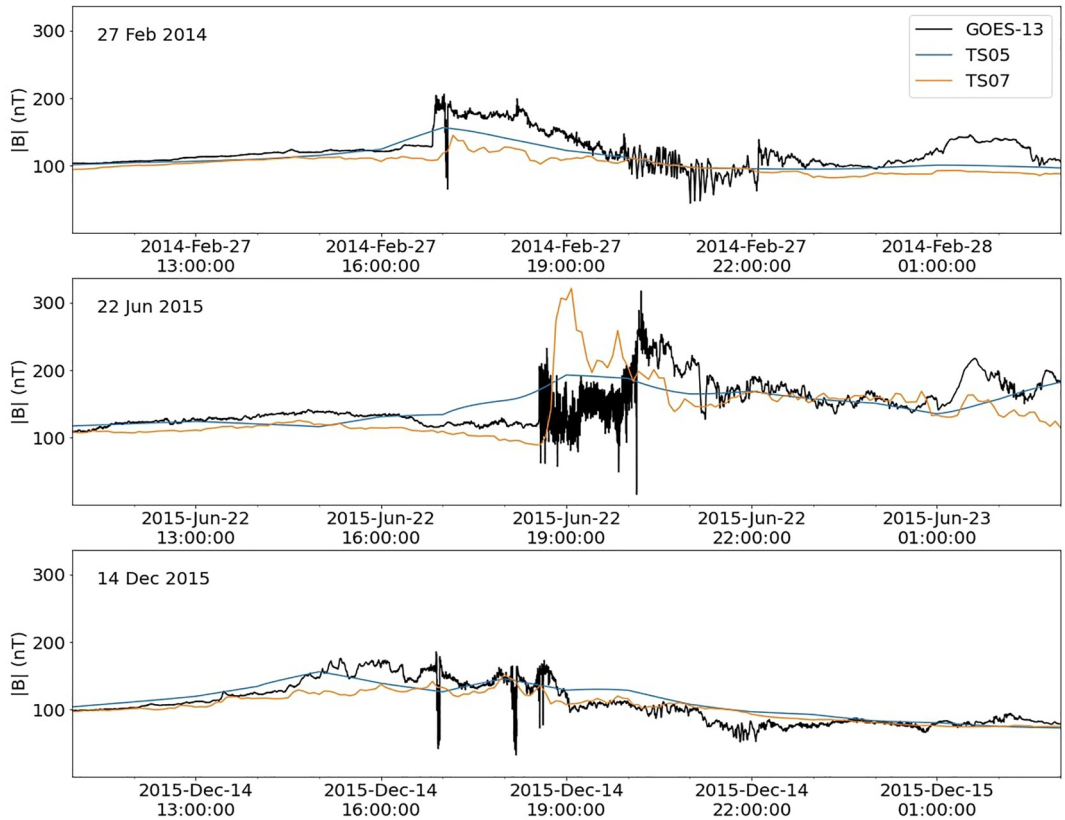


**Figure 4.** A comparison of the magnitude of the magnetic field measured by the GOES-13 satellite with the magnitude of the magnetic field predicted by the TS05 and TS07 external magnetic field models during each of the three events.

same value of the second invariant and uses them to define a drift shell. This method is not energy dependent and does not trace the path of a particle through space. This can also have an effect on the accuracy of crossing predictions, as high energy particles whose guiding centers lie on drift shells just inside the magnetopause may encounter the magnetopause during the course of a gyration and be scattered. We expect the effect of this on the analysis to be small, as the gyroradius of an equatorially mirroring 1 MeV electron near geosynchronous orbit is only on the order of tens of kilometers.

Both the TS05 and TS07 external magnetic field models were unable to reliably predict brief GMCs during the 27 February 2014 and 14 December 2015 events but were able to predict the much longer GMC seen in the 23 June 2015 event. This is likely due to the nature of the external field models, which are statistically fitted to satellite measurements of the external field. TS05 is fitted to 5 min averaged magnetic field data (Tsyganenko & Sitnov, 2005), and TS07 is primarily fitted to 15 min averaged data (Tsyganenko & Sitnov, 2007). This results in smoothing of rapid variations in the field, which in turn result in the field models being unable to capture rapid inward movement of the magnetopause. This can be seen in Figure 4, where the measured field from GOES-13 shows much more rapid variation than either of the field models. While the models match the measured field strength well before the storm onset, in all three events both field models can be seen to underestimate the size of most of the peaks and troughs in the measured field strength and to show far less rapid time variation. Figure 4 also demonstrates why the field models managed to capture the LCDS crossing in the 22 June 2015 event but not in the other two events. The larger and longer lasting change in the measured field strength during the GMC in this event is captured in part by the field models. TS05 fails to capture almost all of the time variation in the field that is shorter than 30 min but captures the overall increase in field strength. TS07 captures more of the shorter time variation, especially after 22:00 on 22 June, but still fails to reproduce the behavior of the field during the GMC. Though this was sufficient to predict a GMC in this event, this behavior suggests that these field models may not reliably predict GMCs, even those lasting over 30 min, as they deviate greatly from even a smoothed time series of the measured field during this event. Both the field models show little to no change

associated with briefer changes in the measured field during the GMCs in the other two events, resulting in the field models returning $L^*$ values during periods when the satellite is on an open drift shell, and its $L^*$ should be undefined. Thus the field models fail to predict GMCs when the associated change in magnetic field is too rapid to be captured by the model.

The Gl14 LCDS used with the British Antarctic Survey Radiation Belt model appears to overestimate the extent to which the LCDS moves inward prior to GMC observations, seen most clearly in panels (E) and (F) of Figure 1, where the LCDS model drops below the $L^*$ values of all three satellites at 13:30 14 December. This is not accompanied by any sign of an LCDS crossing in the electron flux data. This LCDS model is based on the linear relationship between the magnetopause standoff distance and the LCDS from particle tracing simulations, shown in Figure 4 in Matsumura et al. (2011). The simulations in this figure only span a range of magnetopause standoff distances from 7.2 to 9.5$R_E$, and thus extrapolating this relationship to lower altitudes relies on the assumption that the relationship stays in this linear regime. Prior to the storm onsets, while the solar wind pressure is less than 10 nPa and the IMF $B_z$ is not strongly negative, the model magnetopause standoff distance is within the linear regime and the Gl14 LCDS model does remain above the $L^*$ of the geostationary satellites. The lower than expected LCDS values seen in this study suggest that this Gl14 LCDS model should not be considered valid when the magnetopause is significantly lower than 7.2$R_E$.

Observations of the magnetic field at the GOES satellites during GMCs showed that both satellites recorded strongly negative $B_z$ values, sometimes in excess of −150 nT, while outside the magnetopause. This is most evident in panels (C) and (D) in Figure 2. These values are significantly higher than the $B_z$ values recorded at L1 and propagated to the bow shock nose from the OMNIWeb data set. This increase in magnetic field strength close to the magnetopause within the magnetosheath compared to the IMF strength is consistent with the magnetohydrodynamic simulations of Erkaev et al. (2000). These suggest that as the solar wind crosses the bow shock its velocity normal to the magnetopause decreases, and the magnetic pressure increases with decreasing distance to the magnetopause. This can result in magnetic field strength compression ratios of up to 15 between the IMF and the magnetic field directly outside the magnetopause. We have shown that this effect can produce observations by geostationary satellites of strong magnetic fields in directions opposite to that of Earth's magnetic field, sometimes lasting over an hour.

The difference in the profile of an event as observed by satellites at different MLT on the same orbit implies that choice of satellite may have an effect on the output of radiation belt models and forecasts that rely on satellite data to drive them. Specifically, satellites on the nightside see both large variations in flux and occasional highly unphysical $L^*$ values using the TS05 model. Radiation belt models simulating drift averaged fluxes require an outer boundary that properly represents the drift averaged flux along the outermost drift shell. The high degree of MLT dependence in the measurements in the events shown in this study demonstrates that data from a single satellite will be unable to provide an accurate drift averaged outer boundary. The shorter GMCs in these events were comparable to or shorter than 10 min, the drift period of 1 MeV equatorially mirroring electrons at $L = 6.6$. In these cases, losses due to the GMC are likely to be confined to electrons near local noon, with little initial effect on electrons on the nightside. At this time, satellites on the nightside will then see fluxes greater than the average flux on the drift shell and satellites on the dayside will see fluxes lower than the average. In this case of much longer GMCs, such as the one seen in Figure 2, fluxes are expected to drop rapidly at all MLT. Figure 2 demonstrates that a single satellite may still be unable to provide an accurate measure of drift averaged flux at a given drift shell, as the GOES-13 and GOES-15 satellites show large differences in measured flux 4 hr after the event. In this case both field models place both GOES satellites on open drift shells with undefined $L^*$ values for extended periods following and during the GMC. This presents a further difficulty in determining a drift averaged flux as the satellites are not on closed drift shells, and their recorded flux cannot be easily mapped to nearby drift shells.

Greater satellite coverage across a range of MLTs would allow better quantification of the variation in flux observations with MLT, as well as providing the data necessary to determine the drift averaged flux more accurately at nearby drift shells. With additional coverage boundary conditions at a given drift shell for radiation belt models could be generated using a combination of the flux observations from multiple satellites mapped to that drift shell, preferring data from satellites on nearby closed drift shells, and in regions where the field models perform best. Ideally several satellites equipped to measure both flux and the local magnetic field would be spaced out in MLT in geostationary orbit. This would allow better determination of drift averaged fluxes, along with better

data for the validation and fitting of magnetic field models and the ability to calculate the first invariant values of electrons seen by each satellite, which may be used to identify satellites on shared drift shells.

The degree to which differences in observation at different MLT affect modeling of the outer radiation belts requires further investigation to determine, including modeling these events using data from each GOES satellite as an outer boundary and using each LCDS model to account for losses to the magnetopause. Future outer radiation belt modeling work may require developing an appropriate method to combine data from multiple geostationary satellites into a single more representative boundary condition.

## 5. Conclusions

We used data from three satellites in geostationary orbit to analyze flux dropouts caused by GMCs. The data were compared to LCDS models based on the commonly used TS05 and TS07 external field models and to the LCDS model currently used by the British Antarctic Survey Radiation Belt Model. The key findings are summarized here:

1. All events studied showed signs of decreases in flux across a range of $L^*$ values during periods of high magnetopause compression, demonstrating the effects of magnetopause shadowing losses in these events. These losses were all associated with prolonged satellite proximity to the LCDS models, showing that they can be used to effectively predict losses to the magnetopause.
2. Neither the field model based LCDS models, nor the Gl14 LCDS model, were able to predict rapid drops in measured flux caused by brief magnetopause crossings. All three models were able to predict the longer crossing seen in the 22 June 2015 event. A lower bound on the shortest detectable GMC using any of these models would be ≈5 min, a pessimistic upper bound on the shortest detectable GMC would be ≈1 hr. These bounds were determined by looking at the length of the longest GMC that was not predicted (27 February 2014 at 20:00 in Figure 1) and the length of the shortest GMC that was predicted (22 June 2015 at 19:00 in Figure 2).
3. Satellite proximity to noon is a better predictor of which satellites will observe GMCs than satellite $L^*$. Observations made near noon may vary significantly compared to simultaneous observations made only a few hours different in MLT. Consequently, choice of satellite may have a substantial impact on modeling or forecasting even when choosing between satellites with similar orbits.

Current forecasting and reconstruction of the outer radiation belts often rely on data from a single geostationary satellite to produce outer boundary conditions, for example, S. Glauert et al. (2021) using data from GOES-15 to produce the SARIF forecasts. We have shown that data from a single satellite may be unrepresentative of dayside conditions. When data from multiple satellites are available, short timescale forecasts and reconstructions may be improved by using data from a greater number of satellites at a range of MLT values to drive radiation belt models. This demonstrates the value of greater satellite coverage in geostationary orbit in allowing more consistent observations of conditions at all MLTs. Accurate forecasts and reconstructions of short timescale events such as GMCs may require data from at least three geostationary satellites, ideally more.

**Acknowledgments**
We would like to thank Tsutomu Nagatsuma for advice regarding the Himawari-8 SEDA-e data. This material is based upon work supported by the Air Force Office of Scientific Research under award number FA9550-19-1-7039. Richard Horne and Sarah Glauert were supported by the Natural Environment Research Council (NERC) Highlight Topic Grant NE/P01738X/1 (Rad-Sat) and NERC grant NE/V00249X/1 (Sat-Risk) and National and Public Good activity grant NE/R016445/1. Giulio Del Zanna acknowledges support from STFC (UK) via the consolidated grant to the astrophysics group at DAMTP, University of Cambridge (ST/T000481/1). Mervyn Freeman was supported by NSF-NERC grant NE/V015133/1 and NERC grant NE/V002716/1. Adiabatic invariant coordinates were calculated using the IRBEM library, used through the SpacePy python library, accessed via https://github.com/spacepy/spacepy.

## Data Availability Statement

The solar wind parameters used are obtained from the NASA OMNIWeb database (https://omniweb.gsfc.nasa.gov/form/omni_min.html). GOES-13 and GOES-15 data were obtained from NOAA at https://www.ngdc.noaa.gov/stp/satellite/goes/index.html. Data from the Himawari-8 satellite were provided by the NICT HIMAWARI/SEDA database at https://aer-nc-web.nict.go.jp/himawari-seda/. The $L^*$, LCDS and TS05/TS07 magnetic field magnitude data shown in this paper are available from the U.K. Polar Data Centre at https://doi.org/10.5285/346ce427-6663-45e6-b706-285bb79e41ce.

## References

Albert, J. M., Selesnick, R., Morley, S. K., Henderson, M. G., & Kellerman, A. (2018). Calculation of last closed drift shells for the 2013 gem radiation belt challenge events. *Journal of Geophysical Research: Space Physics*, *123*(11), 9597–9611. https://doi.org/10.1029/2018JA025991

Boscher, D., Bourdarie, S., O'Brien, P., & Guild, T. (2013). Irbem Library V4 (Vol. 3, pp. 2004–2008). Retrieved from https://spacepy.github.io/irbempy.html

Capannolo, L., Li, W., Ma, Q., Shen, X.-C., Zhang, X.-J., Redmon, R., et al. (2019). Energetic electron precipitation: Multievent analysis of its spatial extent during emic wave activity. *Journal of Geophysical Research: Space Physics*, *124*(4), 2466–2483. https://doi.org/10.1029/2018ja026291

Capannolo, L., Li, W., Millan, R., Smith, D., Sivadas, N., Sample, J., & Shekhar, S. (2022). Relativistic electron precipitation near midnight: Drivers, distribution, and properties. *Journal of Geophysical Research: Space Physics*, *127*(1), e2021JA030111. https://doi.org/10.1029/2021JA030111
Case, N., & Wild, J. (2013). The location of the Earth's magnetopause: A comparison of modeled position and in situ cluster data. *Journal of Geophysical Research: Space Physics*, *118*(10), 6127–6135. https://doi.org/10.1002/jgra.50572
Erkaev, N. V., Farrugia, C. J., Biernat, H. K., Ogilvie, K., & Quinn, J. (2000). Magnetosheath parameters near the subsolar line predicted by an MHD flow model with anisotropic pressure. *Advances in Space Research*, *25*(7–8), 1523–1528. https://doi.org/10.1016/S0273-1177(99)00665-1
Glauert, S., Horne, R., & Kirsch, P. (2021). Evaluation of sarif high-energy electron reconstructions and forecasts. *Space Weather*, *19*(12), e2021SW002822. https://doi.org/10.1029/2021SW002822
Glauert, S. A., Horne, R. B., & Meredith, N. P. (2014). Simulating the earth's radiation belts: Internal acceleration and continuous losses to the magnetopause. *Journal of Geophysical Research: Space Physics*, *119*(9), 7444–7463. https://doi.org/10.1002/2014JA020092
Glauert, S. A., Horne, R. B., & Meredith, N. P. (2018). A 30-year simulation of the outer electron radiation belt. *Space Weather*, *16*(10), 1498–1522. https://doi.org/10.1029/2018SW001981
Green, J. C., Onsager, T. G., O'Brien, T. P., & Baker, D. N. (2004). Testing loss mechanisms capable of rapidly depleting relativistic electron flux in the Earth's outer radiation belt. *Journal of Geophysical Research*, *109*(A12), A12211. https://doi.org/10.1029/2004ja010579
Loto'Aniu, T., Singer, H., Waters, C., Angelopoulos, V., Mann, I., Elkington, S., & Bonnell, J. (2010). Relativistic electron loss due to ultralow frequency waves and enhanced outward radial diffusion. *Journal of Geophysical Research*, *115*(A12). https://doi.org/10.1029/2010JA015755
Matsumura, C., Miyoshi, Y., Seki, K., Saito, S., Angelopoulos, V., & Koller, J. (2011). Outer radiation belt boundary location relative to the magnetopause: Implications for magnetopause shadowing. *Journal of Geophysical Research*, *116*(A6). https://doi.org/10.1029/2011JA016575
McIntosh, S. W., Chapman, S., Leamon, R. J., Egeland, R., & Watkins, N. W. (2020). Overlapping magnetic activity cycles and the sunspot number: Forecasting sunspot cycle 25 amplitude. *Solar Physics*, *295*(12), 1–14. https://doi.org/10.1007/s11207-020-01723-y
Morley, S. K., Friedel, R. H., Spanswick, E. L., Reeves, G. D., Steinberg, J. T., Koller, J., et al. (2010). Dropouts of the outer electron radiation belt in response to solar wind stream interfaces: Global positioning system observations. *Proceedings of the Royal Society A: Mathematical, Physical & Engineering Sciences*, *466*(2123), 3329–3350. https://doi.org/10.1098/rspa.2010.0078
Nagatsuma, T., Sakaguchi, K., Kubo, Y., Belgraver, P., Chastellain, F., Muff, R., & Otomo, T. (2017). Space environment data acquisition monitor onboard Himawari-8 for space environment monitoring on the Japanese meridian of geostationary orbit. *Earth Planets and Space*, *69*(1), 1–8. https://doi.org/10.1186/s40623-017-0659-6
Olifer, L., Mann, I. R., Morley, S. K., Ozeke, L. G., & Choi, D. (2018). On the role of last closed drift shell dynamics in driving fast losses and Van Allen radiation belt extinction. *Journal of Geophysical Research: Space Physics*, *123*(5), 3692–3703. https://doi.org/10.1029/2018JA025190
Roederer, J. (1970). *Periodic drift motion and conservation of the third adiabatic invariant*. In *Dynamics of Geomagnetically Trapped Radiation* (pp. 72–83). Springer. https://doi.org/10.1007/978-3-642-49300-3_3
Rufenach, C. L., Martin, R., Jr., & Sauer, H. (1989). A study of geosynchronous magnetopause crossings. *Journal of Geophysical Research*, *94*(A11), 15125–15134. https://doi.org/10.1029/JA094iA11p15125
Shprits, Y. Y., Drozdov, A. Y., Spasojevic, M., Kellerman, A. C., Usanova, M. E., Engebretson, M. J., et al. (2016). Wave-induced loss of ultra-relativistic electrons in the Van Allen radiation belts. *Nature Communications*, *7*(1), 1–7. https://doi.org/10.1038/ncomms12883
Shprits, Y. Y., Thorne, R., Friedel, R., Reeves, G., Fennell, J., Baker, D., & Kanekal, S. (2006). Outward radial diffusion driven by losses at magnetopause. *Journal of Geophysical Research*, *111*(A11), A11214. https://doi.org/10.1029/2006JA011657
Shue, J.-H., Song, P., Russell, C., Steinberg, J., Chao, J., Zastenker, G., et al. (1998). Magnetopause location under extreme solar wind conditions. *Journal of Geophysical Research*, *103*(A8), 17691–17700. https://doi.org/10.1029/98JA01103
Staples, F. A., Kellerman, A., Murphy, K. R., Rae, I. J., Sandhu, J. K., & Forsyth, C. (2021). Resolving magnetopause shadowing using multi-mission measurements of phase space density. *Journal of Geophysical Research: Space Physics*, *127*(2), e2021JA029298. https://doi.org/10.1029/2021JA029298
Tsyganenko, N., & Sitnov, M. (2005). Modeling the dynamics of the inner magnetosphere during strong geomagnetic storms. *Journal of Geophysical Research*, *110*(A3), A03208. https://doi.org/10.1029/2004JA010798
Tsyganenko, N., & Sitnov, M. (2007). Magnetospheric configurations from a high-resolution data-based magnetic field model. *Journal of Geophysical Research*, *112*(A6). https://doi.org/10.1029/2007JA012260
Tu, W., Xiang, Z., & Morley, S. K. (2019). Modeling the magnetopause shadowing loss during the June 2015 dropout event. *Geophysical Research Letters*, *46*(16), 9388–9396. https://doi.org/10.1029/2019GL084419
Turner, D. L., Shprits, Y., Hartinger, M., & Angelopoulos, V. (2012). Explaining sudden losses of outer radiation belt electrons during geomagnetic storms. *Nature Physics*, *8*(3), 208–212. https://doi.org/10.1038/nphys2185
Ukhorskiy, A., Sitnov, M., Millan, R., Kress, B., & Smith, D. (2014). Enhanced radial transport and energization of radiation belt electrons due to drift orbit bifurcations. *Journal of Geophysical Research: Space Physics*, *119*(1), 163–170. https://doi.org/10.1002/2013JA019315
Van Allen, J. A., & Frank, L. A. (1959). Radiation around the earth to a radial distance of 107, 400 km. *Nature*, *183*(4659), 430–434. https://doi.org/10.1038/183430a0
Wang, D., & Shprits, Y. Y. (2019). On how high-latitude chorus waves tip the balance between acceleration and loss of relativistic electrons. *Geophysical Research Letters*, *46*(14), 7945–7954. https://doi.org/10.1029/2019GL082681
Wrenn, G. L. (1995). Conclusive evidence for internal dielectric charging anomalies on geosynchronous communications spacecraft. *Journal of Spacecraft and Rockets*, *32*(3), 514–520. https://doi.org/10.2514/3.26645
Yu, Y., Koller, J., & Morley, S. (2013). Quantifying the effect of magnetopause shadowing on electron radiation belt dropouts. *Annales geophysicae*, *31*(11), 1929–1939. https://doi.org/10.5194/angeo-31-1929-2013,2013